JMolMed

ORIGINAL ARTICLE

Manic Fringe promotes endothelial-to-mesenchymal transition mediated by the Notch signalling pathway during heart valve development

Junjie Yang[1,2] · Zhi Wang[2] · Yue Zhou[2] · Shiwei Jiang[2] · Xiji Qin[2] · Zhikang Xu[2] · Yu Wang[1,2] · Mengying Zuo[2,3] · Zhuo Meng[2] · Sun Chen[2] · Qingjie Wang[2] · Jian Wang[2] · Kun Sun[1,2]

Abstract

A fundamental event in the formation of heart valves involves the transformation of endocardial cells within the outflow tract (OFT) and atrioventricular canal (AVC) cushions through a process known as endothelial-to-mesenchymal transition (EndMT). Aberrant EndMT is a primary cause of congenital valvular malformations. Manic Fringe (MFNG) has been previously associated with cardiovascular development, although its role in heart valve development remains underexplored. In this study, we seek to enhance our understanding of MFNG's involvement in valve formation and its association with EndMT. Staining results of histological section revealed the expression of MFNG in the AVC and OFT from embryonic day 9.5 to 10.5 (E9.5–E10.5), when EndMT takes place. Cellular data demonstrated that MFNG exerts a positive regulatory influence on the EndMT process, promoting endothelial cell (EC) migration by enhancing the activity of the Notch signalling pathway. MFNG knockdown mediated by antisense morpholino oligonucleotides (MO) injection caused abnormal development of the heart and valves in zebrafish. Furthermore, through whole-exome sequencing (WES), we identified a heterozygous MFNG mutation in patients diagnosed with tetralogy of Fallot-pulmonary valve stenosis (TOF-PS). Cellular and molecular assays confirmed that this deleterious mutation reduced MFNG expression and hindered the EndMT process. In summary, our study verifies that MFNG plays a role in promoting EndMT mediated by the Notch signalling pathway during the heart and valve development. The MFNG deleterious variant induces MFNG loss of function, potentially elucidating the underlying molecular mechanisms of MFNG's involvement in the pathogenesis of congenital heart valve defects. These observations contribute to our current genetic understanding of congenital heart valve disease and may provide a potential target for prenatal diagnosis and treatment.

Key messages

- Our examination revealed, for the first time, that MFNG exhibited high expression levels during EndMT of heart valve development in mice.
- Our findings provide compelling evidence that MFNG plays a role in promoting EndMT mediated by the Notch signalling pathway.
- Our results identified, for the first time, a deleterious MFNG p. T77M variant that inhibited the EndMT process by downregulating the activity of the Notch signalling pathway, thereby preventing the normal valve formation. MFNG may serve as an early diagnostic marker and an effective therapeutic target for the clinical treatment of congenital heart valve defects.

Junjie Yang, Zhi Wang, and Yue Zhou contributed equally to this article.

Extended author information available on the last page of the article

🖄 Springer

Introduction

Cardiac valve defects are significant contributors to morbidity and mortality during the perinatal and neonatal periods and represent the most prevalent subset of cardiovascular malformations, accounting for over 50% of congenital cardiovascular defects [1]. These congenital valvular issues are integral components of complex cardiovascular conditions, including pulmonary valve stenosis (PS) in tetralogy of Fallot (TOF) and aortic valve stenosis (AS) in hypoplastic left heart syndrome (HLHS) [2], both of which can have dire consequences. Despite their high incidence, treatment options for congenital heart valve defects remain limited and generally exhibit unfavorable long-term prognoses [3].

It is well established that the development of heart valves commences with the EndMT process, which becomes most pronounced around E9.5 in mice [4–6]. Aberrant EndMT can lead to congenital valvular malformations [7]. During this process, the endocardial cells within the AVC and OFT change when stimulated by adjacent cardiomyocytes, reducing cell–cell connections and initiating EndMT [8]. Many previous studies have shown that the major molecular mechanisms governing zebrafish cardiac valve formation are quite similar to those found in mammalian hearts. The first phase of heart valve formation in the zebrafish is that the endocardial cells at the AVC undergo the EndMT process, which occurs at 36 h post-fertilization (hpf). The endocardial cells at the AVC proliferate and extend into the cardiac jelly at 80 hpf to contribute to the formation of cushion, and then, cardiac cushion begins its morphogenetic rearrangement at 105 hpf to form the mature valve leaflets [9]. EndMT is characterized by the gradual transformation of ECs, which lose their typical characteristics and take on mesenchymal traits under stimulation [10, 11]. These transformed cells acquire a spindle-shaped, elongated morphology and gain mobility and invasive capabilities due to the loss of cell–cell junctions [10–12]. Multiple signalling pathways, including the classical TGFβ signalling pathway and the Notch signalling pathway, are involved in regulating EndMT-associated valve formation, with the Notch pathway playing a crucial role in the heart valve development [13, 14].

Development of heart valves is a complex process involving interactions among various cell types and intricate genetic programs [15–18]. Mounting evidence exhibits the genetic basis of congenital valvular malformations [2, 16, 19]. Notable mutations such as G296S in GATA4 contribute to pulmonary valve abnormalities, as observed in a mouse model carrying this human mutation, which results in pulmonary valve stenosis (PS) [20–23]. Variants in NOTCH1 and SMAD6 are linked to bicuspid aortic valve (BAV) and have been found to have functional deficiencies in vitro, and

targeted GATA5 deletion in mice leads to a partially BAV phenotype [24–29].

MFNG, a member of the glycosyltransferase family, plays a central role in modulating Notch signalling. It introduces N-acetylglucosamine (GlcNAc) into the O-fucosylated EGF-like regions of Notch receptors, promoting the binding of Delta ligands to Notch receptors and inhibiting the binding of Jagged ligands to Notch receptors [30–32]. Previous studies have shown that MFNG facilitates ventricular trabeculae formation, ventricular maturation, and compaction during embryonic mouse development [33, 34]. However, the connection between MFNG and heart valve development has not been adequately elucidated.

In this investigation, our examination revealed that MFNG exhibited high expression levels during the embryonic development of heart valves in mice. Subsequent in vitro experiments further confirmed MFNG's role in promoting the EndMT process, underlining its significant association with heart valve formation. MFNG has also been shown to play a crucial role in zebrafish embryonic heart valve development. Moreover, recent advances in our understanding of the mechanisms governing heart valve development, alongside improved human genome sequencing techniques, have unveiled numerous genetic factors contributing to congenital heart valve disease in humans. To ascertain the pivotal role of MFNG in the heart valve development, we conducted a study involving patients diagnosed with TOF-PS. To identify MFNG variants, these individuals underwent WES. Remarkably, we detected one pathogenic MFNG mutation in these patients. This MFNG variant was found to alter mRNA and protein expression levels, consequently inhibiting the EndMT process by downregulating the Notch signalling pathway. These findings provide compelling evidence that the MFNG variant plays a significant role in the development of congenital valvular defects. Hence, we have successfully confirmed that MFNG is intricately involved in the regulation of the EndMT process, mediated by the Notch signalling pathway, during heart valve development.

Methods

Study population and DNA extraction

In this study, we enrolled 40 patients diagnosed with TOF-PS and 60 patients diagnosed with pulmonary atresia with ventricular septal defect (PA-VSD), confirmed by both cardiac echocardiography and evaluation performed by a specialist cardiologist. Additionally, 120 unrelated healthy controls without congenital heart valve defects were recruited from Shanghai Xin Hua Hospital. All participants in the

patient cohort were members of the Chinese Han community, ranging in age from newborns to 17 years. DNA extraction was performed according to the standard protocol, employing the QIAamp DNA Blood Mini Kit (QIAGEN, Germany). The study design adhered to the principles of the Declaration of Helsinki.

WES, Sanger sequencing, and variant analysis

WES was conducted on all samples utilizing the Illumina HiSeq 2500 platform to screen for mutations. Nonsynonymous variations in the encoding regions of MFNG, with a frequency of less than 0.1% in normal control individuals (i.e., less than 0.1% in the 120 healthy participants and publicly available variation databases, including ExAC), were considered. To further validate the candidate MFNG variant, Sanger sequencing was employed. In this study, rare mutations were defined as those with a minor allele frequency (MAF) less than 0.5%. The pathogenicity of the MFNG mutation was assessed using various bioinformatic websites, including SIFT (http://sift.jcvi.org/www/SIFT_enst_submit.html), Mutation Taster (http://www.mutationtaster.org/), PolyPhen-2 (http://genetics.bwh.harvard.edu/pph2/), and CADD (https://cadd.gs.washington.edu/info).

Conservation analysis of MFNG protein sequence

MFNG protein sequences from various species, including *Homo sapiens* (human), *Mus musculus* (house mouse), *Rattus norvegicus* (rat), *Macaca mulatta* (rhesus monkey), *Bos taurus* (cattle), and *Pan troglodytes* (chimpanzee), were obtained from NCBI (https://www.ncbi.nlm.nih.gov/protein/). The Clustal X software (http://www.clustal.org) was utilized to assess the conservation of MFNG protein sequences.

Plasmids and site-specific mutagenesis

A full-length human MFNG ORF was inserted into the pCDH-CMV-MCS-EF1-copGFP-T2A-Puro vector to construct the wild-type (WT) MFNG expression plasmid. To introduce mutations, the QuikChange XL site-directed mutagenesis kit (Stratagene, La Jolla, CA, USA) was employed. All plasmids were subjected to verification for integrity and accuracy via Sanger sequencing.

Cell culture, transient transfection, and treatment

Human umbilical endothelial cells (HUVECs) from passages four to seven were cultured in Dulbecco's Modified Eagle's Medium (DMEM, Invitrogen, CA, USA), supplemented with 10% fetal bovine serum (MP Biomedicals, USA) and 1% penicillin–streptomycin solution (Gibco, USA). Transfections were performed by separately introducing 3 µg of empty vector, oe-MFNG, and oe-MUT plasmids into HUVECs using FuGene HD (Promega, USA) when the cell concentration in the 6-well plate reached 70–80%. After 24 or 48 h of transient transfection, HUVECs were harvested for subsequent experiments. To induce EndMT in vitro, HUVECs were treated with transforming growth factor beta 2 (TGFβ2, 10 ng/ml, R&D, 302-B2) for 48 h as the treatment group, or with 0.1% bovine serum albumin (BSA) for 48 h as the control group when they reached 70–80% confluence. HUVECs were starved with basal medium for 12–16 h before treatment, and the medium with TGFβ2 or 0.1% BSA was freshly replaced every day. Additionally, DAPT (Sigma-Aldrich, St. Louis, CA, USA) was added to the cell medium (20 µg/ml) and renewed every other day to inhibit the Notch pathway.

Lentivirus assembly and transduction

To stably overexpress MFNG in HUVECs, the pCDH vector containing human MFNG (pCDH-MFNG) was constructed. After synthesizing the MFNG overexpression lentiviral vector, a mixture of psPAX2, pMD2.G, and the modified pCDH-CMV-MCS-EF1-copGFP-T2A-Puro containing the MFNG coding sequence was co-transfected into Hek-293 T cells at a ratio of 4:2:1. Polyethyleneimine (PEI) was used for transfection at a ratio of 3:1 (PEI µg: total DNA µg). The viral supernatants were collected at 48 and 72 h and filtered through a 0.45-µm filter. Subsequently, HUVECs were transduced with the lentivirus at a 1:1 ratio of viral supernatants to fresh medium, supplemented with 8 µg/ml polybrene. After 48 h of incubation, 2 µg/ml puromycin was added to the culture medium to select for transfected cells. To knock down MFNG in HUVECs, recombinant lentiviruses carrying MFNG-targeting small interfering RNA (sh-MFNG) were designed and synthesized. The lentiviral transfer vector (pLKO.1-TRC) was constructed, and sh-MFNG expression was driven by the U6 promoter. Lentivirus packaging and cell transfection followed previously established protocols.

Wound healing assay

HUVECs were seeded into 6-well plates at a density of 5×10^5 cells per well. When the cells reached approximately 95% confluence, they were serum-starved for 16 h. Subsequently, cell monolayers were scratched using 200-µl pipette tips and washed three times with PBS. The cells were then incubated with fresh medium containing 1% FBS for 24 h, and images were captured at 0 and 24 h after scratching. ImageJ software was used to analyze the wound area healing.
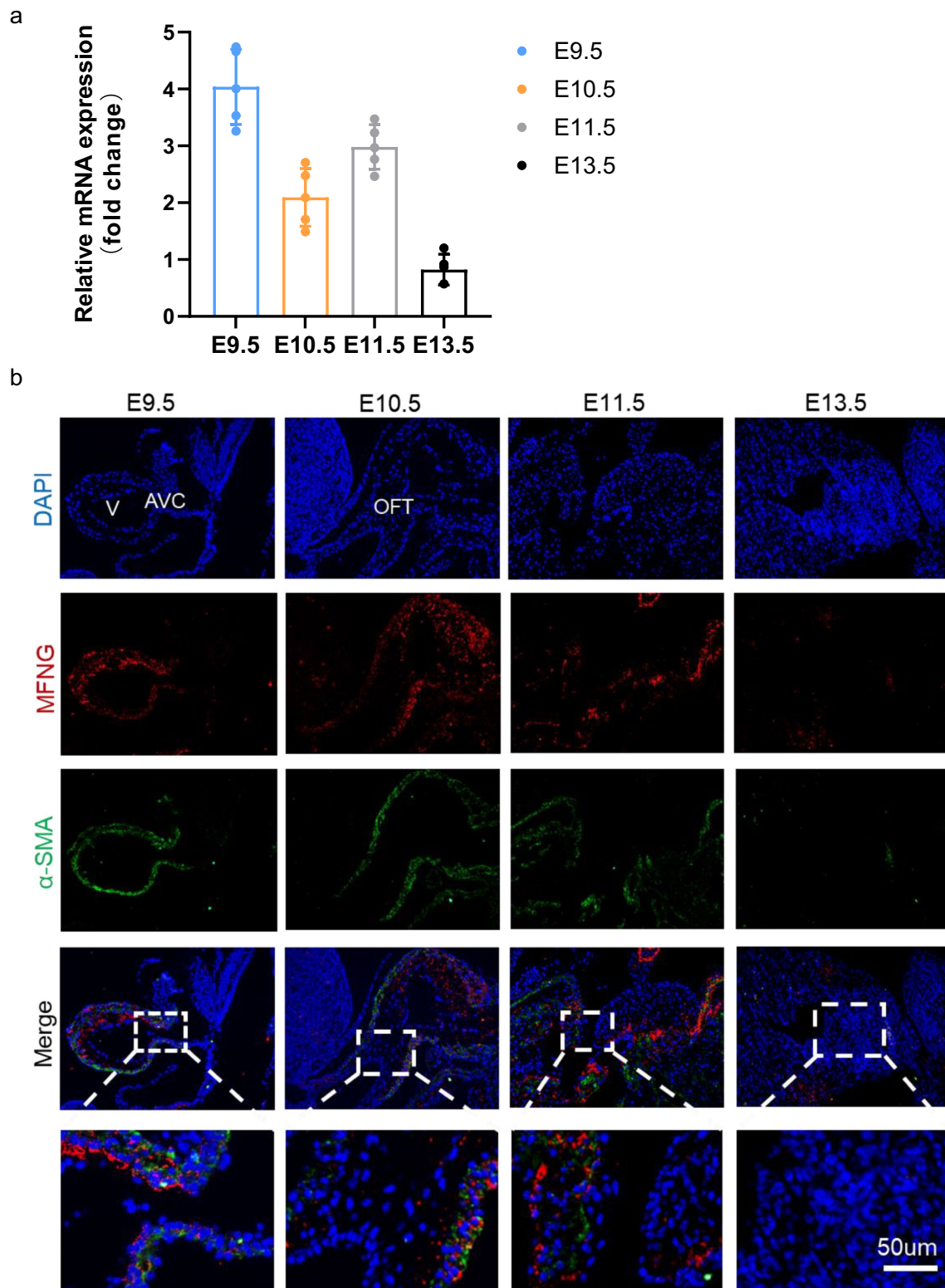
Fig. 1 Expression of MFNG in mice during embryonic heart development. **a** qRT-PCR analysis of MFNG mRNA levels during the embryonic heart development of mice. GAPDH served as an internal reference. **b** Immunofluorescence staining revealed the endogenous distribution of MFNG at E9.5–E11.5 and E13.5 in mouse embryos. Scale bars = 50 μm. All data presented here were obtained from five independently repeated biological experiments
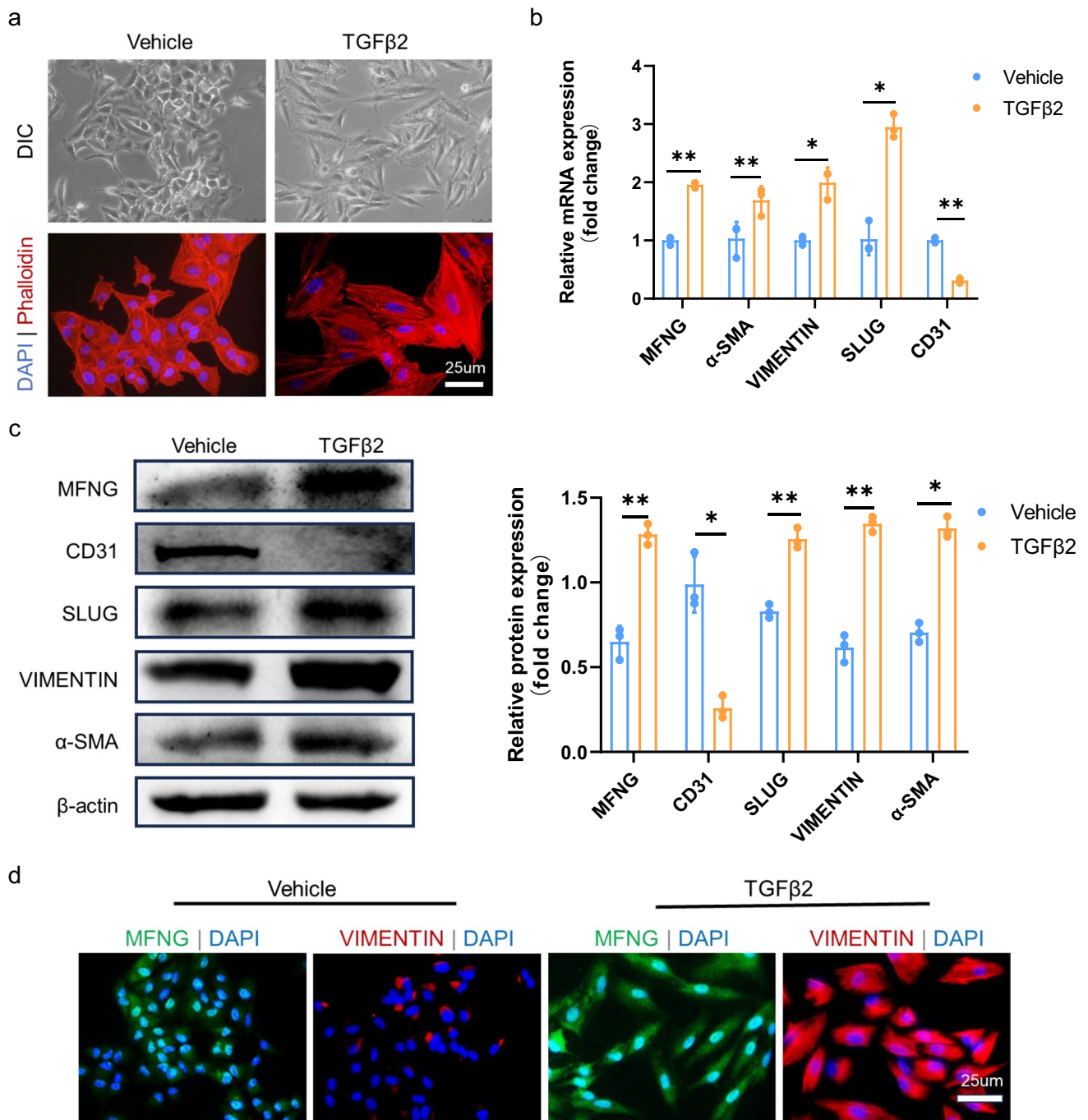
Fig. 2 Upregulation of MFNG in TGFβ2-induced EndMT. **a** The transition of HUVECs from their typical cobblestone-like shape to spindle-like cells with protrusions after 48 h of exposure to 10 ng/ml TGFβ2 was visualized under a light microscope (upper). F-actin staining with phalloidin revealed elongated HUVECs with protrusions. Scale bars = 25 μm. **b** qRT-PCR analysis was used to estimate the relative mRNA levels of MFNG, α-SMA, VIMENTIN, SLUG, and CD31 in HUVECs. GAPDH was employed as a loading control. **c** Western blot displayed the alterations in protein levels of EndMT-specific markers and MFNG following a 48-h treatment with 10 ng/ml TGFβ2. β-actin was used as a loading control. The band density of MFNG, CD31, SLUG, VIMENTIN, and α-SMA on the Western blot was quantified using ImageJ software. **d** Cellular immunofluorescence demonstrated a significant upregulation of MFNG expression in HUVECs after TGFβ2 treatment. Scale bars = 25 μm. All data reported here were obtained from three independently repeated biological experiments
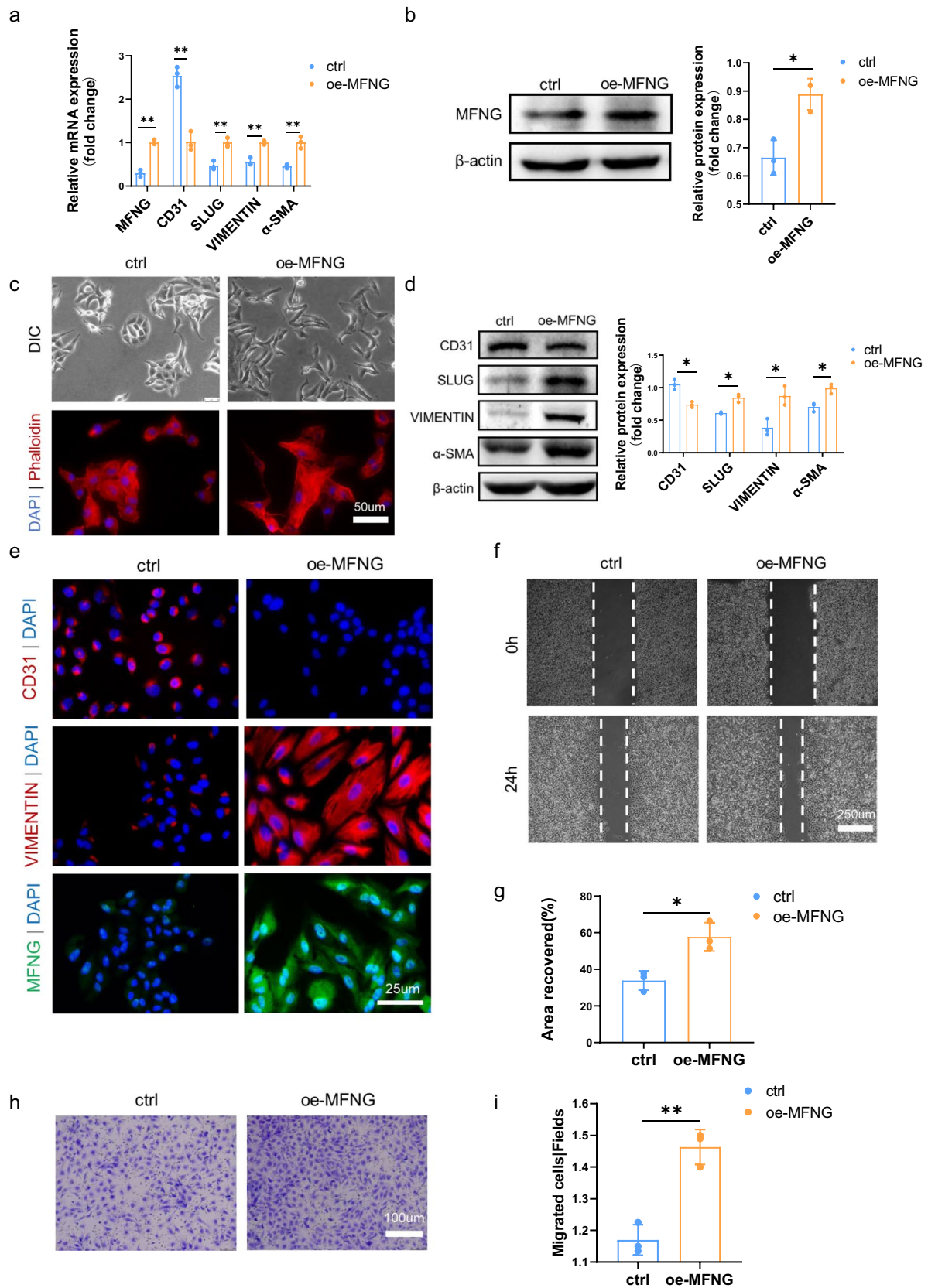
◄**Fig. 3** Induction of EndMT by MFNG overexpression in HUVECs. **a** qRT-PCR analysis was conducted to determine the relative mRNA levels of MFNG, with GAPDH as the loading control. **b** Western blot confirmed MFNG overexpression in HUVECs, with β-actin as the loading control. The band density of MFNG was quantified. **c** Light microscopy (upper) illustrated the morphological changes in HUVECs after MFNG overexpression. F-actin staining with phalloidin using a fluorescence microscope (lower) revealed the transformation of HUVECs into mesenchymal stellate cells with long protrusions and filopodia 48 h post-transfection. Scale bars = 25 μm. **d** Western blot depicted alterations in EndMT-related markers in HUVECs with MFNG overexpression compared to the control group, with a quantitative analysis of the relative protein expressions of MFNG, CD31, SLUG, VIMENTIN, and α-SMA using ImageJ software. **e** Cellular immunofluorescence staining for CD31 (red), VIMENTIN (red), and MFNG (green). Nuclei were counterstained with DAPI. Scale bars = 25 μm. **f**, **g** Representative images of cell wound healing assays and quantification of the scratch repair rate. Scale bars = 250 μm. **h**, **i** Assessment of the migratory ability of HUVECs overexpressing MFNG via the transwell assay and quantification of migrated HUVECs. Scale bars = 100 μm. All data presented are from three independently repeated biological experiments

Transwell assay

Samples with 2×10^5 cells were resuspended in a serum-free culture medium after trypsinization and plated on the upper layer of transwell chambers (Corning, USA). The residue cells on the upper side migrated toward the lower chamber with a gradient of 20% FBS. The cells on the top surface of the membrane were wiped out, leaving only the cells with the ability to migrate. These cells were washed three times with PBS, fixed with 4% paraformaldehyde (PFA) for 15 min, and stained with crystal violet for 30 min after 24 h of incubation. The inverted microscope was used to capture the images of migrated cells.

Quantitative real-time PCR

Total RNA was extracted from HUVECs and reverse transcribed into cDNA using a reverse transcriptase kit (TaKaRa, Japan). Quantitative real-time PCR (qRT-PCR) was performed on the Applied Biosystems 7500 system using SYBR Green (TaKaRa, Japan). GAPDH was used as an internal reference. The qRT-PCR settings were as follows: 3 min at 50 °C and 30 s at 95 °C, followed by 40 cycles of 10 s at 95 °C and 30 s at 60 °C. The relative gene expression was quantified using the ΔΔCt calculation method. The specific primer sequences are listed in supplementary Table 1.

Western blot

HUVECs were collected by scraping and lysed with RIPA buffer (Beyotime, P0013B) containing a mixture of protease and phosphatase inhibitors (PMSF, 1:100) for 30 min on ice. Protein concentration was determined using the BCA protein quantification kit (Beyotime, P0010). Equal amounts of protein from each group were separated by SDS-PAGE and transferred to an NC membrane. After blocking with 5% skim milk for 1.5 h at room temperature, the membranes were incubated overnight at 4 °C with specific primary antibodies. Subsequently, the membranes were incubated with secondary antibodies conjugated to horseradish peroxidase (HRP) for 1.5 h at room temperature. Gel images were captured using the Tanon gel imaging system, and each band was normalized to the loading control β-actin. Immunoblots were analyzed by densitometry using ImageJ software.

Cellular and tissue immunofluorescence staining

For cellular staining, HUVECs cultured on coverslips were fixed in 4% PFA for 15 min. Subsequently, they were permeabilized with 0.5% Triton X-100 in PBS for 10 min and then blocked with 5% BSA for 1.5 h at room temperature. Following the removal of the blocking buffer, the primary antibody diluted in the blocking buffer was applied to the HUVECs and incubated overnight at 4 °C. The next day, HUVECs were exposed to fluorescence-conjugated secondary antibodies for 1.5 h at room temperature to visualize the specific target protein. After the secondary antibody incubation, DAPI (Vector Laboratories, USA) with an anti-fluorescence quenching agent was used to stain cell nuclei. For staining of tissue sections, paraffin-embedded heart tissue sections were dewaxed in xylene and rehydrated through a graded alcohol series: 100% ethanol, 90% ethanol, 75% ethanol, and distilled water. Antigen retrieval was performed by heating in sodium citrate buffer (pH = 6) for 6 min, followed by cooling to room temperature. The steps for permeabilization of tissue sections, blocking with 5% BSA, and subsequent incubation with primary and secondary antibodies were the same as those described for cells. Finally, a fluorescence microscope was used to detect red, green, and blue channels.

Maintenance of zebrafish, microinjection of morpholinos into the embryos, and hematoxylin–eosin staining

The Tg (myl7: EGFP) transgenic line embryos labelled with green fluorescence were purchased from the China Zebrafish Resource Center and maintained at 28.5 °C under standard laboratory conditions. All the experiments received approval from the Animal Care and Use Committee of Xinhua Hospital. Morpholino antisense oligos (MO), chemically modified oligonucleotides, can cause aberrant splicing by targeting splice junctions. They remain effective in blocking protein synthesis of the targeted gene(s) for
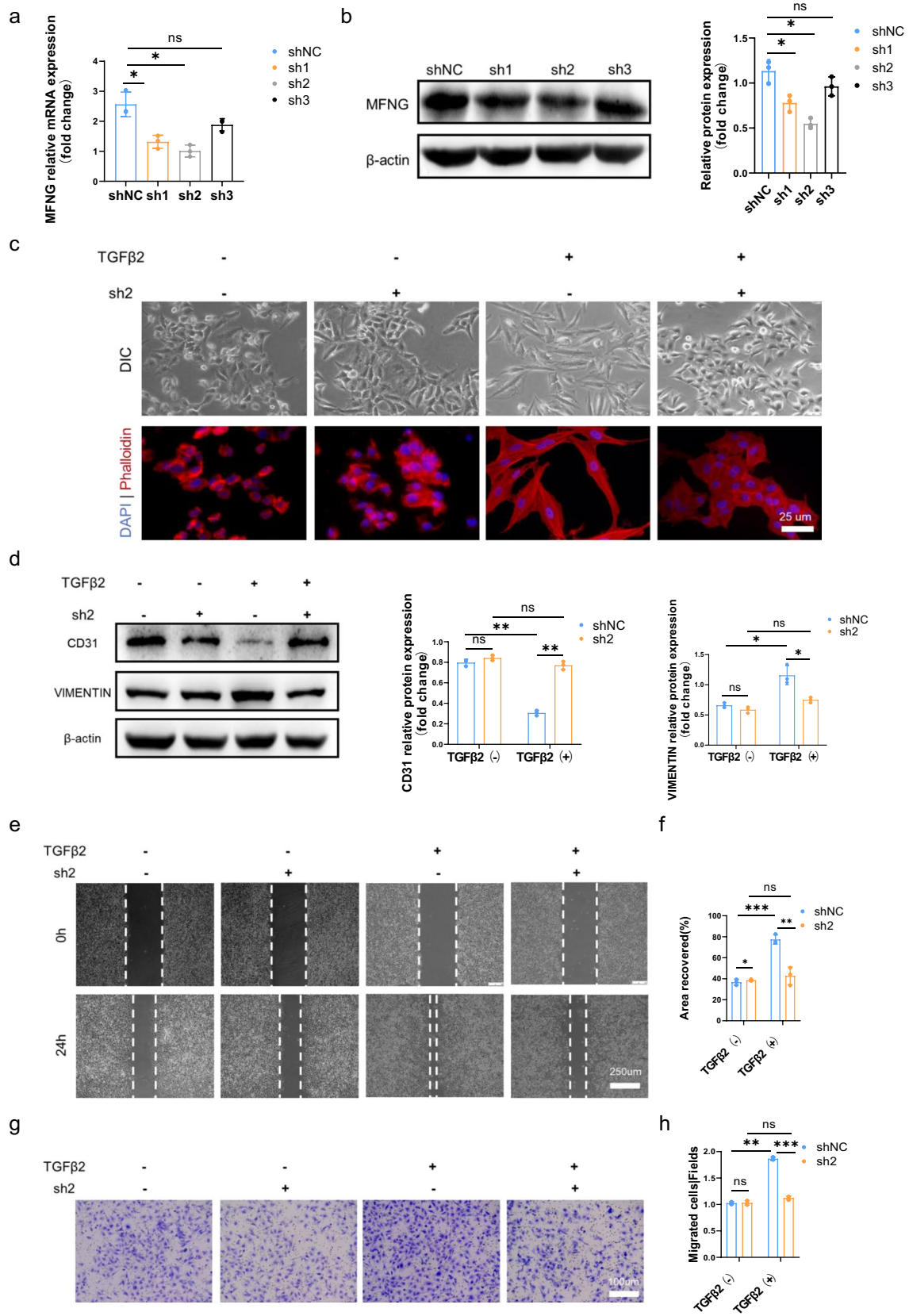
◄**Fig. 4** Attenuation of TGFβ2-induced EndMT in HUVECs by MFNG deprivation. **a** Verification of the knockdown efficiency of three MFNG-targeted shRNAs with different interference sequences at the transcriptional level. **b** Western blot confirmed successful MFNG knockdown in HUVECs, with corresponding quantitative analysis. β-actin served as the loading control. **c** Representative images illustrating the endothelial morphological phenotype of HUVECs transduced with MFNG shRNA lentivirus. The morphology of HUVECs infected with equal doses of sh-NC and sh-MFNG differed in response to TGFβ2. MFNG knockdown in HUVECs blocked the morphological changes induced by TGFβ2. Scale bars = 25 μm. **d** Western blot displayed alterations in EndMT markers, along with corresponding quantitative analysis. β-actin was used as an internal control. **e–h** MFNG deprivation hindered TGFβ2-induced HUVEC migration. **e, f** Representative images of cell wound healing assays and quantification of the scratch repair rate. Scale bars = 250 μm. **g, h** The transwell migration assay was performed, and the relative number of migrated cells per high-power field was measured. Scale bars = 100 μm. All data reported are from three independently repeated biological experiments

3–4 days. Zebrafish MFNG MO1 (5′-AGCACCATTAGC TTACTCACTTTTT-3′) and MO2 (5′-ATGAATAGATGT GATACTGACCGTC-3′) were designed and synthesized by Gene Tools (OR, USA). A standard control MO (5′-CCTCTTACCTCAGTTACAATTTATA-3′) was employed as a negative control. For knockdown assays, MO were injected into the yolk sac of embryos when they were at the 1–2 cell stage using a pressure microinjection device (PICOSPRITZER® III, Parker, USA). qRT-PCR analysis of MFNG cDNA collected from the whole embryos 30 h after the injection was employed to confirm MO efficiency. The preliminary experiment was then carried out to evaluate the appropriate injection concentration of MO. The embryos were examined periodically, and their phenotypes within each group were recorded at 72 hpf. Zebrafish embryos were fixed in 4% PFA, followed by dehydration through a graded ethanol series, clearing in xylene, and embedding in paraffin wax. Longitudinal sections of 4 μm thickness were dewaxed, dried, and stained with hematoxylin and eosin (HE) according to standard protocols. The resulting images were acquired using a Leica microscope.

In vitro OFT explant culture and isolation of ECs from the OFT explants

The cultures of the OFT explants were carried out in accordance with the previously described methodology. The rat tail collagen-type I matrices (Corning, 354236) were allowed to polymerize in an incubator set at 37 °C and 5% CO2. The OFT tissue was dissected in sterile PBS from E10.5 embryos. The OFT cushions were exposed by using sharp tweezers and secured with the cushion-side facing downwards on the collagen gels, which were allowed to facilitate the attachment of the cushions. After overnight adhesion, adenoviral infections were performed to analyze the effects

of MFNG overexpression and mutation on the OFT explants. To express MFNG or MFNG mutation, the OFT explants were infected with adenovirus containing either MFNG (AdV-MFNG) or the MFNG mutation (AdV-MUT), which were tagged with GFP, or empty adenovirus (AdV-GFP). Endocardial cells that underwent transformation were identified as the spindle-shaped cells that migrated away from the explants or invaded the gel. Bright-field images and GFP fluorescence images of OFT explants were obtained using a Leica microscope. Explants were fixed and stained with α-SMA to detect mesenchymal cells. Cell numbers were determined by manual counting. The ECs isolated from the OFT explants were collected for further research after infection with AdV-MFNG, AdV-MUT, or AdV-GFP and subsequent removal of the myocardial tissue using collagenase type II (Sigma-Aldrich).

Statistical analysis

All measurement data were analyzed using GraphPad Prism 8 and presented as the mean ± standard error (SEM). The experiments were independently repeated at least three times. The statistical significance of observed differences was assessed using a two-tailed t-test between the two groups. One-way analysis of variance (ANOVA) with Tukey's multiple comparison test when more than two groups are compared. Two-way ANOVA was used to test for differences between groups with multiple factors. For zebrafish MO assays, the chi-squared test (and Fisher's exact test) was applied to compare the proportions of zebrafish embryonic phenotypes between the ctrl-MO group and the MFNG-MO group. A p-value less than 0.05 was considered significant.

Results

MFNG was observed in both endocardial and mesenchymal cells within the AVC and OFT of the mouse heart during the E9.5–E11.5 developmental stage

The most intense EndMT occurs during the E9.5 to E11.5 developmental stage, which plays a pivotal role in the embryonic heart valve development of mice. Despite previous studies not associating MFNG with heart valve development, our qRT-PCR analysis was conducted to investigate MFNG expression throughout mouse embryonic heart valve development (Fig. 1a). The results revealed that at the transcriptional level, MFNG expression peaked at E9.5 and gradually declined till E13.5. To gain further insights into the spatiotemporal distribution of MFNG, immunofluorescence analysis was performed on normal mouse embryos (Fig. 1b). This analysis confirmed the presence of MFNG
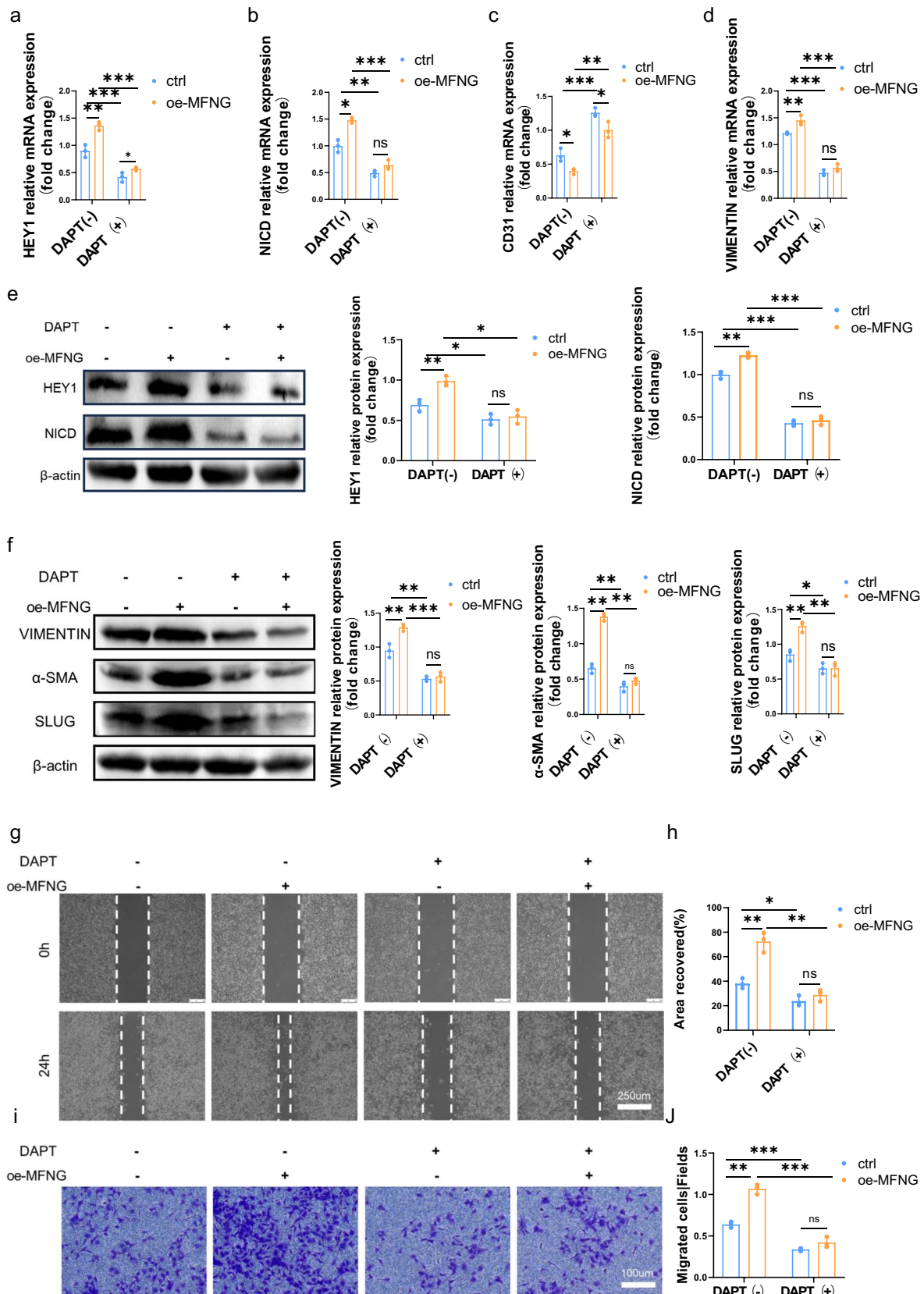
◄**Fig. 5** MFNG promoted EndMT by upregulating the activity of Notch signalling pathway. **a–d** Transcriptional analysis revealed that HUVECs overexpressing MFNG exhibited increased expression of Notch pathway molecules such as HEY1 and NICD, along with elevated levels of EndMT-associated genes, including VIMENTIN. Conversely, CD31 expression was restored following DAPT treatment. GAPDH was utilized as an internal reference for these evaluations. **e**, **f** Western blot analysis, represented by the accompanying blots and quantitative data, confirmed these findings at the protein level, illustrating alterations in EndMT markers and Notch pathway molecules. β-actin served as the loading control. **g**, **i** Cell migration capabilities were assessed through wound healing and transwell assays. **h** Quantitative analysis of wound area healing was conducted using ImageJ software. **j** The quantification of cell migration ability was performed by counting cells per field. All data presented are the result of three independently repeated biological experiments

in the endocardial and mesenchymal cells of the AVC and OFT at E9.5–E11.5 in mice, indirectly suggesting a potential association between MFNG and the EndMT process during heart valve development.

MFNG was upregulated in a cellular EndMT model

The process of EndMT is characterized by alterations in endothelial cell morphology, molecular markers, and cellular functionality. Changes in cell polarity and significant cytoskeletal reorganization lead to morphological shifts. The expression of EndMT-specific genes and the corresponding proteins in endothelial cells change at both transcriptional and translational levels. Additionally, endothelial cells undergoing EndMT exhibit enhanced motility and increased migratory potential. To assess the occurrence of EndMT from these three perspectives, we used TGF-β2, a well-established regulator of the EndMT process, to induce EndMT in HUVECs as an in vitro model. Following treatment with TGFβ2 for 48 h, HUVECs underwent a morphological transformation from cobblestone-like endothelial cells to spindle-shaped mesenchymal cells, indicating their enhanced motility (Fig. 2a). qRT-PCR and Western blot analyses revealed downregulation of endothelial cell marker (CD31) and upregulation of mesenchymal markers (α-SMA and VIMENTIN) and SLUG at both transcriptional and translational levels following TGFβ2 induction (Fig. 2b, c), confirming the successful establishment of an in vitro EndMT model. We also observed an upregulation of MFNG expression during TGFβ2-induced EndMT, which was further validated by qRT-PCR and Western blot (Fig. 2b, c). Immunofluorescence staining results provided additional evidence of altered cell morphology, with significant increases in VIMENTIN and MFNG expression (Fig. 2d). These findings confirm the upregulation of MFNG during the EndMT process and suggest its role in modulating EndMT.

MFNG acted as a positive regulator of EndMT

To further investigate the role of MFNG in the activation of EndMT, both gain-of-function and loss-of-function strategies for MFNG were employed. Lentiviral transfection was conducted for 2 days, followed by a 2-day puromycin selection to obtain positive cells. The efficiency of the transfection was assessed at both the transcriptional (Figs. 3a and 4a) and translational levels (Figs. 3b and 4b), revealing successful MFNG overexpression, and the highest knockdown efficiency was achieved with shMFNG-2. HUVECs overexpressing MFNG exhibited typical stromal cytoplasmic extensions and cytoskeletal rearrangements (Fig. 3c). Conversely, MFNG depletion in HUVECs attenuated the TGFβ2-induced EndMT when compared to sh-NC groups, as evidenced by the morphological changes of HUVECs (Fig. 4c).

Furthermore, our data showed that MFNG overexpression led to a significant downregulation of endothelial markers and upregulation of mesenchymal markers and SLUG at both the transcriptional (Fig. 3a) and translational levels (Fig. 3d). In line with these observations, MFNG depletion suppressed TGFβ2-induced EndMT, as reflected by the changes in EndMT-related markers (Fig. 4d). Cellular immunofluorescence after MFNG overexpression confirmed typical variations in HUVEC cell morphology and changes in protein markers associated with EndMT (Fig. 3e). These findings collectively affirmed that MFNG acts as a positive regulator of EndMT. Lastly, the impact of MFNG overexpression and depletion on cell migration was assessed using scratch and transwell assays (Figs. 3f, g and 4e, f and Figs. 3h, i and 4g, h, respectively), confirming that MFNG facilitates the EndMT process. These experiments provide further evidence crucial role of MFNG in EndMT.

MFNG possessed the critical function in the EndMT via Notch signalling pathway

Numerous prior studies have established that MFNG can modulate the Notch signalling pathway by altering their ligand-binding specificity during development. Furthermore, activation of the Notch signalling in endothelial cells leads to significant changes in morphology, phenotype, and function, indicative of mesenchymal transformation. In light of this, we sought to investigate whether lentivirus-mediated overexpression of MFNG in HUVECs influences the EndMT process through the Notch signalling pathway. As depicted in Fig. 5a and b, MFNG overexpression resulted in a substantial increase in mRNA levels of HEY1 and NICD (the cleaved and activated form of Notch) compared to the control groups. To effectively inhibit the Notch pathway activation, we employed the potent Notch pathway inhibitor, DAPT, and
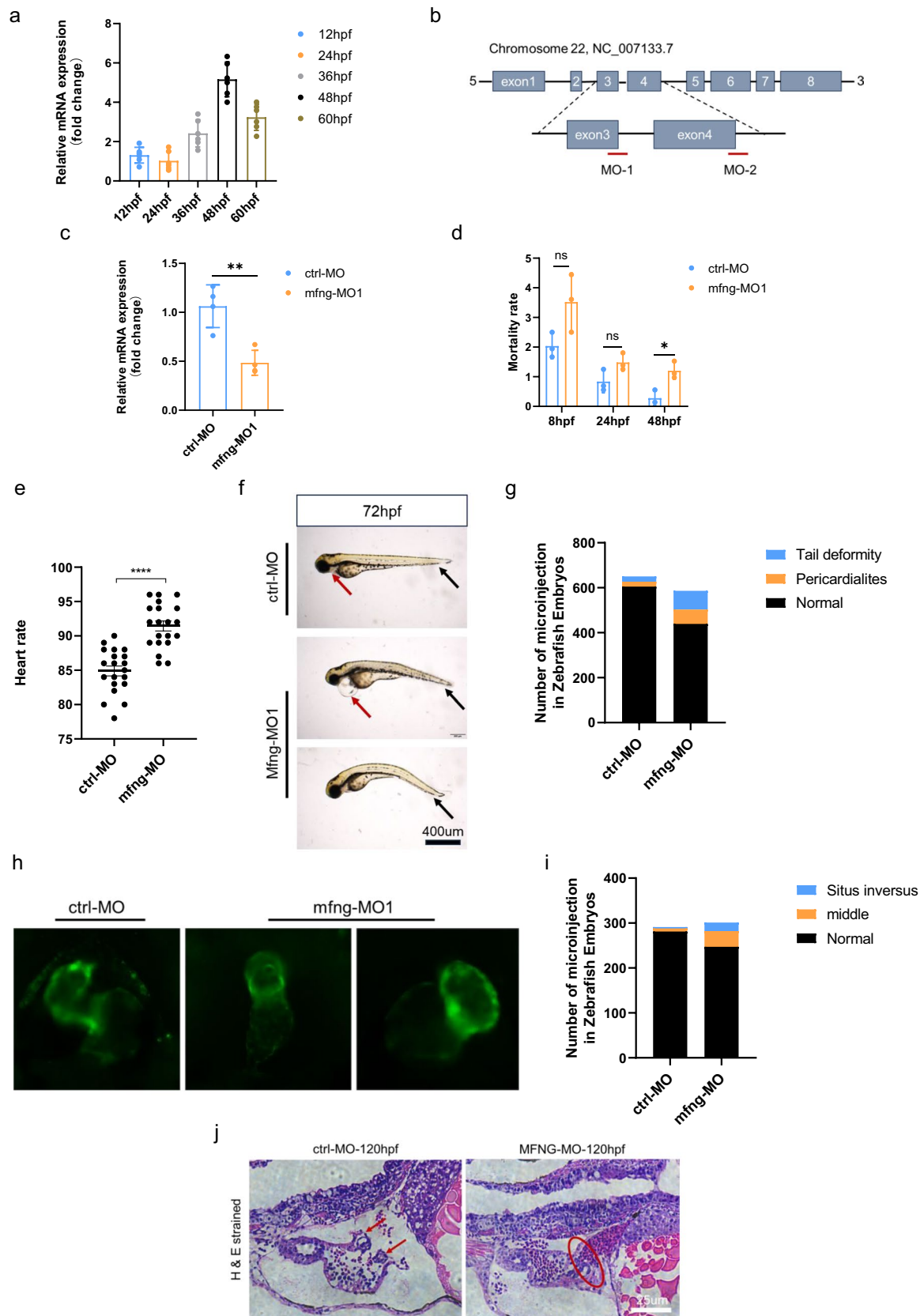
◄**Fig. 6** MFNG role in zebrafish is fundamental for heart and valve development. **a** qRT-PCR analysis of the relative transcript level of MFNG during embryogenesis from 24 to 60 hpf. Data are shown as the mean ± SEM, $n = 6$. **b** Schematic representation of MFNG exons with the target sites of MFNG MO-1 and MFNG MO-2, which induce MFNG deficiency in zebrafish embryos by targeting the 3-exon–3-intron junction and the 4-exon–4-intron junction, respectively. **c** The efficacy of MFNG MO1 was confirmed by qRT-PCR. Data are presented as mean ± SEM, $n = 4$. **d** The lethality of ctrl-MO and MFNG-MO embryos from 8 to 48 hpf. The chi-square test was used for statistical analysis. **e** The heart rate of ctrl-MO and MFNG-MO embryos at 72 hpf. **f** Bright-field views of live ctrl-MO and MFNG-MO embryos at 72 hpf. Note the pericardial edema (red arrowhead) and tail deformity (black arrowhead). **g** Compared to the ctrl-MO group, the MFNG-MO group exhibited a significantly higher number of pericardial edema and tail deformities. **h**, **i** Lateral views of ctrl-MO embryos and MFNG-MO embryos at 72 hpf, captured in the Tg (myl7: EGFP) background. Zebrafish embryos in the MFNG-MO group displayed absent regular heart looping. The chi-square test was used for statistical analysis. **j** Sections of zebrafish embryos stained with HE at 120 h post-MO injection. In the MFNG-MO group, the valve leaflets observed in the ctrl-MO group are absent. The red arrow represents the heart valve, and the red oval denotes the atrioventricular boundary

observed a significant reduction in Notch signalling pathway activity at the mRNA level, irrespective of the presence of MFNG overexpression (Fig. 5a, b). These findings were corroborated at the translational level by Western blot results, which showed that MFNG upregulated the expression of markers associated with the Notch pathway, thus enhancing Notch signalling pathway activation (Fig. 5e). To further investigate whether MFNG promotes EndMT through the Notch signalling pathway, we employed DAPT to inhibit Notch pathway activation. We observed that the promoting effect of MFNG on EndMT was attenuated following the blockade of Notch signalling pathway, at both the mRNA (Fig. 5c, d) and protein expression levels (Fig. 5f). Finally, the scratch assay (Fig. 5g, h) and the transwell assay (Fig. 5i, j) demonstrated that MFNG overexpression facilitated cell migration and invasion. Intriguingly, the migratory and invasive capabilities of HUVECs were reduced after DAPT treatment. In summary, we have substantiated that the Notch signalling pathway is, at the very least, partially downstream of MFNG, and these data suggest that MFNG promotes the EndMT process by activating the Notch signalling pathway.

Table 1 Frequency and spectrum of patients with congenital heart valve defects in this study

| Diagnoses	Number	Percentage (%)	Age
TOF-PS	40	40%	1 month–13 years
PA-VSD	60	60%	3 months–12 years
Total	100	100%	1 month–13 years

TOF-PS TOF with pulmonary valve stenosis, *PA-VSD* PA with ventricular septal defect

**Table 2** Clinical information and mutations of MFNG in patients with congenital heart valve defects

Patient ID	Gender	Age (year)	Cardiac phenotype	Location in gene	Function	Nucleotide change	Amino acid change	SIFT	Mutation taster	PolyPhe2_HDIV	1000 genomes allele frequency	ExAC_ALL allele frequency
82	F	1	TOF|PS	Exon1	nonsynonymous SNV	c.C230T	p.T77M	0 (D)	1.0 (D)	1.0 (D)	-	0

The standard of each scoring software is SIFT software score ≤ 0.05 (harmful), > 0.05 (harmless); mutation taster gives a judgment of the risk of mutation, divided into "disease-causing" and "polymorphism"; PolyPhen-2 score < 0.5 (Benign), > 0.5 (possibly damaging); the closer the score is to 1, the higher the risk of disease (probably damaging)

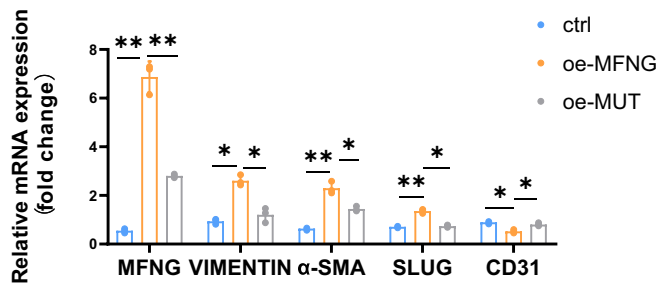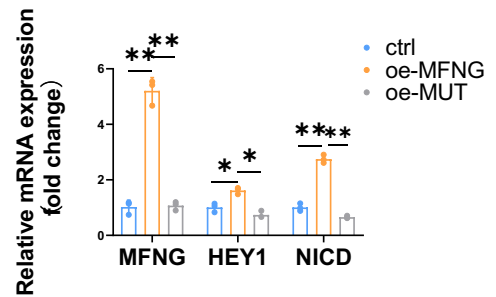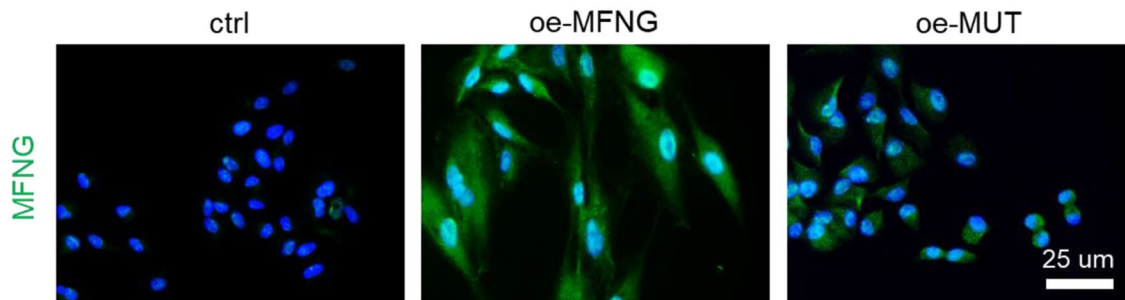*F* female, *TOF* tetralogy of Fallot, *PS* pulmonary valve stenosis
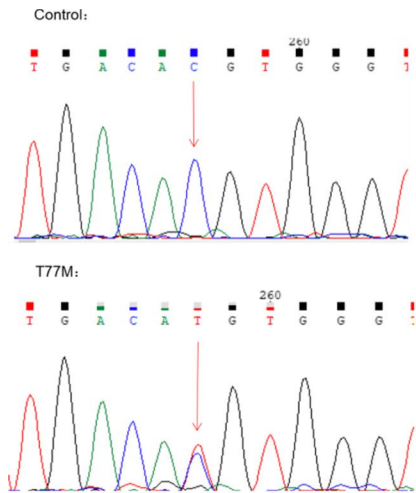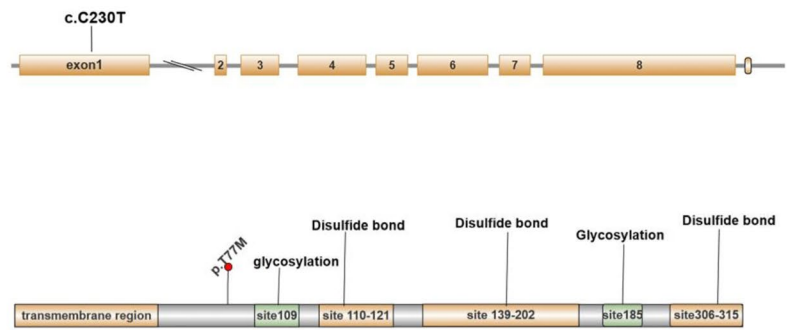
◀**Fig. 7** Validation and in silico analysis of the MFNG variant. **a** Sequences showing the MFNG missense variant, identified in both patients and healthy controls, with arrows indicating heterozygous nucleotide changes. **b** Depiction of the MFNG gene's exon and protein structure, highlighting the location of the genetic variation within this study. Exon 1 of MFNG harbored the base substitutions. The amino acids were primarily composed of glycosylation and disulfide bond domains. **c** The MFNG mutation was found to exhibit a high degree of conservation across vertebrates, as evidenced by the Clustal X alignment of the MFNG protein in various species. Stars indicate identical residues. In our study, human umbilical vein endothelial cells (HUVECs) served as the control group. HUVECs transfected with the MFNG wild-type plasmid were designated as the overexpression group (oe-MFNG), while HUVECs transfected with the MFNG mutant plasmid were designated as the mutant group (oe-MUT). **d, e** The relative mRNA expression of MFNG, genes associated with EndMT, and molecules related to the Notch pathway in HUVECs subjected to various treatments was meticulously assessed, employing GAPDH as a reference gene. Significantly distinct mRNA expression levels of MFNG, EndMT-related genes, and Notch pathway molecules were evident when comparing the oe-MFNG and oe-MUT groups. **f** Cellular immunofluorescence staining underscored the diminished expression of MFNG in the oe-MUT groups compared to the oe-MFNG groups, as visualized through microscopic images. Scale bars = 25 μm

MFNG knockdown mediated by splice-blocking MO injection leads to abnormal heart development and absence of valve structure in zebrafish

To investigate the effects of MFNG on heart and valve development in zebrafish, the expression profile of MFNG during zebrafish development was first investigated by qRT-PCR analysis. The results showed that MFNG mRNA levels elevated from 24 to 48 hpf, peaking at 48 hpf, a critical stage in zebrafish embryonic heart valve development, and then decreased at 60 hpf (Fig. 6a). Thus, MFNG was expressed in the developing embryonic heart valves, consistent with our previous findings in mice. To investigate the function of MFNG at different stages of heart development, MO1 and MO2 were separately injected into Tg (myl7: EGFP) transgenic embryos expressing endogenous EGFP. The knockdown efficiency of MO1 and MO2 was confirmed by qRT-PCR. Our data indicated that MO1 had a higher knockdown efficiency compared to MO2. Consequently, MO1 was selected for injection into the yolk sac of embryos to observe the resulting phenotype (Fig. 6b, c; SI1). Compared to the ctrl-MO embryos, MFNG-MO embryos showed a higher lethality, with a statistically significant difference observed between the two groups at 48 hpf (Fig. 6d). In addition, the MFNG-MO group displayed severe pericardial edema, tail deformity, abnormal heart rate, and absent regular heart looping at 72 hpf, distinguishing them from the ctrl-MO group (Fig. 6e–i). Further analysis using hematoxylin and eosin staining of zebrafish hearts at 120 h post-MO injection revealed that, compared to the ctrl-MO group, the valve leaflets in the

MFNG-MO group failed to form properly (Fig. 6j). Taken together, these observations reveal that MFNG knockdown disrupts both heart and valve development, leading to a lethal phenotype.

A pathogenic heterozygous MFNG variant was identified in patients with TOF-PS

The development of abnormal heart valves is commonly observed in complex congenital cardiovascular conditions, such as pulmonary valve stenosis, which represents the most severe phenotype of TOF. In our study, we identified a pathogenic heterozygous variant of the MFNG gene in 40 patients with TOF-PS through WES. We meticulously ruled out any influence from other known pathogenic genes, and it is important to note that we did not find any MFNG mutations in the 120 healthy controls (Table 1). The specific MFNG variant, denoted as p.T77M, resulted in amino acid substitutions and was predicted to be deleterious based on assessments by various bioinformatics software tools such as SIFT, PolyPhen-2, and Mutation Taster (Table 2). As depicted in Fig. 7a, the candidate mutation in the MFNG gene was validated through Sanger sequencing chromatograms. Figure 7b illustrates that the MFNG variant is located in exon 1, with the amino acid substitution occurring in close proximity to the glycosylation domain. Moreover, multiple sequence alignments of the MFNG protein across various vertebrates, as presented in Fig. 7c, revealed a high degree of conservation at the amino acid substitution site, underscoring the potential functional consequences of this alteration in the MFNG protein.

The MFNG variant inhibited the EndMT process via the Notch pathway

To gain further insights into the impact of the MFNG mutation on the EndMT process through the Notch signalling pathway, we conducted an in-depth assessment of the consequences on both aspects. Our findings, as validated through qRT-PCR (Fig. 7d, e) and Western blot analysis (Fig. 8a), indicated that the MFNG mutation resulted in a downregulation of its expression. This decrease in MFNG expression was corroborated by cellular immunofluorescence results (Fig. 7f). In contrast to the overexpression group, the mutated group exhibited a significant increase in the expression of endothelial markers, along with a decrease in mesenchymal markers and SLUG at both the mRNA and protein levels (Figs. 7d and 8a). Furthermore, the MFNG variant was associated with the suppression of molecules connected to the Notch signalling pathway (Figs. 7e and 8b). OFT explants were microdissected from wild-type hearts at E10.5 and infected with green fluorescent protein (GFP)-tagged adenovirus containing MFNG
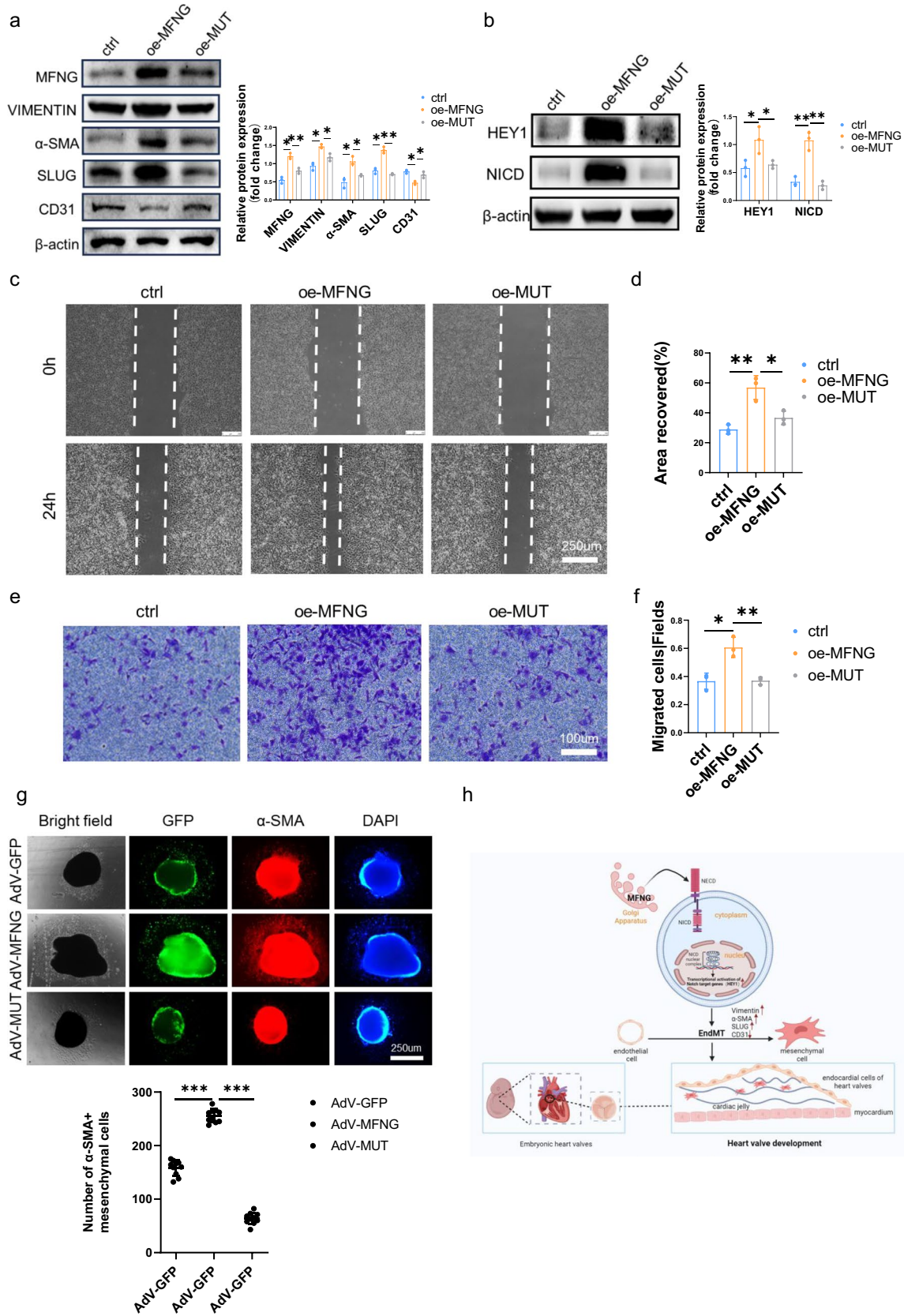
◄**Fig. 8** MFNG mutation blocked EndMT by inhibiting Notch pathway. **a**, **b** To delve deeper, we conducted an examination of the relative protein expression of MFNG, EndMT-related markers, and molecules associated with the Notch pathway in HUVECs subjected to various treatments, with Western blot analysis. The intensity of protein expression was quantified using ImageJ software, normalized to β-actin expression. Additionally, we conducted representative experiments, such as cell **c** wound healing assays and **e** transwell assays, which provided visual evidence that the MFNG variant had a restraining effect on the migration capacity of HUVECs. Quantitative statistics for cell wound **d** healing assays and **f** transwell assays (f) were also included. It is worth noting that all data presented here were derived from three independently repeated biological experiments. **g** Bright-field images demonstrate mesenchymal cell outgrowth from adenovirus-infected explants. GFP fluorescent images represent all cells infected with adenovirus. The mesenchymal cells migrating from endothelial cells were marked with the α-SMA antibody (red). The cell nuclei were stained with DAPI, which produces a blue signal. The quantitative analysis results demonstrate a significant reduction in the number of migrating mesenchymal cells in the presence of the MFNG mutation. High magnification results are shown in Fig. SI3. **h** A schematic model of the mechanisms of MFNG-mediated heart valve formation. MFNG exerts a positive regulatory influence on the EndMT process by enhancing the activity of the Notch signalling pathway, thereby promoting the heart valve development

(AdV-MFNG), MFNG mutation (AdV-MUT), or empty adenovirus (AdV-GFP). The endothelial cells (ECs) isolated from OFT explants were pooled for qRT-PCR and Western blot analysis. The results were consistent with those obtained from HUVECs (Fig. SI2). Our experiments utilizing scratch and transwell assays (Fig. 8c–f) demonstrated that the MFNG mutation hindered the migration ability of HUVECs. Finally, the potential roles of the MFNG mutation in the EndMT process during OFT development were investigated. Our results show that the AdV-MUT-infected OFT explants exhibited a markedly diminished capacity for migration compared to the AdV-MFNG-infected OFT explants (Fig. 8g). The number of α-SMA-positive mesenchymal cells of outgrowth was quantified for each OFT sample (Fig. 8g), and we observed that a significant reduction in AdV-MUT samples compared to the AdV-GFP samples. These results strongly suggest that the MFNG variant downregulates the activity of the Notch signalling pathway, consequently inhibiting the EndMT process. Furthermore, MFNG is necessary for cell migration during endocardial cushion formation.

Discussion

While previous studies have indicated the potential involvement of MFNG in vertebrate cardiovascular development, its role in heart valve development has remained relatively uncharted. Our investigation uncovered elevated MFNG expression in endothelial and mesenchymal cells within the AVC and OFT during the crucial E9.5–E11.5 stage of murine embryonic development. Subsequent cellular and molecular experiments strongly indicated that MFNG upregulates Notch signalling activity, thereby promoting the EndMT process. In addition, MFNG knockdown via MO in zebrafish caused a higher lethality, severe pericardial edema, heart looping disorder, and absence of valve structure in zebrafish. Consequently, our findings represent the first evidence of a connection between MFNG and the Notch signalling pathways during heart valve development.

Fringe proteins, a group of 40 kDa type II membrane proteins, are abundantly localized in the Golgi apparatus [35–37], and they belong to the beta-1,3-N-acetyl-glucosaminyltransferases (GlcNAcTs) [32, 38]. MFNG's crucial role in cardiovascular development is well established. During ventricular development, the temporal and spatial specificity of Notch receptor-ligand interactions is intricately regulated by MFNG. Positioned in the ventricular endocardium, MFNG facilitates Delta signalling to activate endocardial Notch1 between mouse embryonic day E8.5–10.5, significantly contributing to cardiomyocyte proliferation and trabecular growth. Interestingly, a reduction in MFNG levels after E11.5 tilts the balance toward Jagged signalling to Notch1, resulting in the formation of functional ventricular wall [33]. Furthermore, MFNG and Dll4 co-expression is observed in endothelial cells of coronary vessels during mouse embryonic day E13.5–E15.5, potentially enhancing MFNG's role in augmenting Dll4 signalling to Notch. Significantly, enforced MFNG expression interferes with arterio-venous differentiation, coronary plexus remodelling, and perivascular cell maturation at E16.5 [39]. However, MFNG's potential involvement in heart valve development has remained inadequately explored.

Furthermore, MFNG has been implicated as a regulator of the epithelial-to-mesenchymal transition (EMT) [32], prompting us to investigate its role in this critical process during heart valve formation. We observed that MFNG was highly expressed in the endocardial and mesenchymal cells of the AVC and OFT at E9.5–E11.5, pivotal sites and phases in EndMT events during heart valve development [40]. This intriguing finding strongly suggested that MFNG is intimately linked to heart valve formation. Our cellular experiments shed light on the mechanism by which MFNG influences cardiac valve development. Surprisingly, MFNG upregulated mesenchymal markers and enhanced the migration capability of endothelial cells, aligning with its role in promoting a claudin-low breast cancer phenotype through facilitating migration. Hence, our gain and loss-of-function experiments collectively indicate that MFNG may exert positive regulatory control over the occurrence and development of EndMT. Consequently, our work underscores the indispensable role of MFNG in modulating EndMT-associated valve development.

Endocardial cells undergo the EndMT process, which is a transformative phenomenon essential for the development of cardiac septa and valves [41]. Numerous signalling pathways contribute to the initial establishment and specification of EndMT in heart valves, such as the BMP, TGF-β, and Notch signalling pathways [4, 42, 43]. However, the intricate mechanisms governing their activation and suppression remain incomplete. It has been documented that the Fringe family of glycosyltransferases can modulate the Notch signalling pathway by elongating carbohydrates within the Notch extracellular domain (NECD). Consequently, we embarked on an exploration of MFNG's impact on the Notch signalling pathway to unveil the underlying mechanism by which MFNG promotes EndMT. By scrutinizing the transcriptional and translational levels of molecules linked to the Notch pathway and EndMT following the substantial expression of MFNG, we discovered that MFNG overexpression heightened Notch signalling activity, thereby propelling the EndMT process. Furthermore, even in the presence of MFNG overexpression, when Notch signalling was obstructed, the EndMT process and the migratory capability of endothelial cells were impeded. In sum, our data substantiate that MFNG plays an active role in regulating EndMT and cell migration during heart valve formation by enhancing Notch signalling activity.

The zebrafish has been used as a model organism and is a powerful tool to model human heart and valve development due to its rapid organogenesis and optical accessibility [44]. It has been reported that knocking down the MEIS2 ortholog in zebrafish results in a cardiac morphogenesis phenotype, including a smaller and non-looping heart [45]. Knocking out tnni1b in zebrafish results in the defects of atrioventricular valve development [46]. To investigate the role of MFNG in heart and valve development in vivo, MFNG was knocked down by injecting MO into zebrafish embryos. Our results suggest, for the first time, that the normal function of MFNG may be essential for embryonic heart and valve development.

Prior research has definitively established the involvement of genetic factors in regulating heart valve development by impacting the EndMT process [47–49]. To provide further clarity on the association between MFNG and heart valve development, we performed WES to identify the MFNG variant in 40 TOF-PS patients, revealing a potentially disease-causing mutation. This mutation was predicted to be deleterious by various bioinformatics software. Additionally, in an in vitro transfection assay, we confirmed that this mutation reduced MFNG expression and inhibited the EndMT process. Furthermore, the MFNG mutation suppressed Notch signalling activity, suggesting that MFNG mutation may hinder heart valve development by reducing Notch activity. This study furnishes the initial evidence supporting the notion that MFNG pathogenic heterozygous mutations may participate in regulating human congenital heart valve developmental malformations.

MFNG belongs to the beta-1,3N-acetylglucosaminyltransferases (GlcNAcTs) family [38]. Glycosyltransferases perform a vital regulatory role in glycosylation, a pivotal biological mechanism governing protein structure and stability [32]. MFNG has the capacity to modify Notch signalling by elongating O-linked fucose residues within the Notch receptor EGF-like domains [50], thereby altering Notch-Delta/Jagged affinity and impacting the Notch pathway's activity [34, 40, 50]. Regrettably, our study did not focus on elucidating how the MFNG variant influences the glycosylation process.

In conclusion, our results present the first evidence of the involvement of MFNG in heart valve development. MFNG exhibited high expression in both endocardial and mesenchymal cells situated within the AVC and OFT endocardial cushions during the E9.5–E11.5 period in mice. Our cellular experiments demonstrated that MFNG can enhance EndMT by elevating the activity of the Notch signalling pathway. MFNG knockdown via MO in zebrafish caused abnormal heart and valve development. Furthermore, the identification of MFNG pathogenic mutations in patients with congenital heart valve developmental defects, along with cell transfection experiments confirming that the MFNG variant inhibits EndMT by reducing Notch signalling pathway activity, indicates that MFNG could be a novel susceptibility gene for congenital heart valve defects. Thus, the pivotal role of MFNG in EndMT significantly influences the pathogenesis of these EndMT-related heart valve defects.

Abbreviations OFT: Outflow tract; AVC: Atrioventricular canal; EndMT: Endothelial-to-mesenchymal transition; MFNG: Manic Fringe; EC: Endothelial cell; MO: Antisense morpholino oligonucleotides; WES: Whole-exome sequencing; TOF-PS: Tetralogy of Fallot-pulmonary valve stenosis; HPF: Hours post-fertilization; GlcNAc: N-Acetylglucosamine; HUVEC: Human umbilical vein endothelial cell; BSA: Bovine serum albumin; PEI: Polyethyleneimine; PFA: Paraformaldehyde; qRT-PCR: Quantitative real-time polymerase chain reaction

Data availability All data related to the study are included in the article. For additional information, please contact the corresponding author according to reasonable request.

Declarations

Ethical approval and consent to participate All experimental methods were carried out in accordance with the approved guidelines and regulations. Human peripheral blood samples were collected on a voluntary basis, and written informed consent was obtained from the participants or their legal guardians. These human studies received approval from the Medical Ethics Committee of Xinhua Hospital (No. XHEC-F-2017–004).

Competing interests The authors declare no competing interests.

References

1. Go AS, Mozaffarian D, Roger VL, Benjamin EJ, Berry JD, Borden WB, Bravata DM, Dai S, Ford ES, Fox CS et al (2013) Heart disease and stroke statistics–2013 update: a report from the American Heart Association. Circulation 127(1):e6–e245. https://doi.org/10.1161/CIR.0b013e31828124ad

2. Pierpont ME, Basson CT, Benson DWJR, Gelb BD, Giglia TM, Goldmuntz E, McGee G, Sable CA, Srivastava D, Webb CL (2007) Genetic basis for congenital heart defects: current knowledge: a scientific statement from the American Heart Association Congenital Cardiac Defects Committee, Council on Cardiovascular Disease in the Young: endorsed by the American Academy of Pediatrics. Circulation 115(23):3015–38. https://doi.org/10.1161/circulationaha.106.183056

3. Virani SS, Alonso A, Benjamin EJ, Bittencourt MS, Callaway CW, Carson AP, Chamberlain AM, Chang AR, Cheng S, Delling FN et al (2020) Heart disease and stroke statistics-2020 update: a report from the American Heart Association. Circulation 141(9):e139–e596. https://doi.org/10.1161/cir.0000000000000757

4. Combs MD, Yutzey KE (2009) Heart valve development: regulatory networks in development and disease. Circ Res 105(5):408–21. https://doi.org/10.1161/circresaha.109.201566

5. Fishman MC, Chien KR (1997) Fashioning the vertebrate heart: earliest embryonic decisions. Development 124(11):2099–117. https://doi.org/10.1242/dev.124.11.2099

6. O'Donnell A, Yutzey KE (2020) Mechanisms of heart valve development and disease. Development 147(13):dev183020. https://doi.org/10.1242/dev.183020

7. von Gise A, Pu WT (2012) Endocardial and epicardial epithelial to mesenchymal transitions in heart development and disease. Circ Res 110(12):1628–45. https://doi.org/10.1161/circresaha.111.259960

8. Person AD, Klewer SE, Runyan RB (2005) Cell biology of cardiac cushion development. Int Rev Cytol 243:287–335. https://doi.org/10.1016/s0074-7696(05)43005-3

9. Chen IH, Wang HH, Hsieh YS, Huang WC, Yeh HI, Chuang YJ (2013) PRSS23 is essential for the snail-dependent endothelial-to-mesenchymal transition during valvulogenesis in zebrafish. Cardiovasc Res 97(3):443–53. https://doi.org/10.1093/cvr/cvs355

10. Bischoff J (2019) Endothelial-to-mesenchymal transition. Circ Res 124(8):1163–1165. https://doi.org/10.1161/circresaha.119.314813

11. Kovacic JC, Dimmeler S, Harvey RP, Finkel T, Aikawa E, Krenning G, Baker AH (2019) Endothelial to mesenchymal transition in cardiovascular disease: JACC state-of-the-art review. J Am Coll Cardiol 73(2):190–209. https://doi.org/10.1016/j.jacc.2018.09.089

12. Piera-Velazquez S, Jimenez SA (2019) Endothelial to mesenchymal transition: role in physiology and in the pathogenesis of human diseases. Physiol Rev 99(2):1281–324. https://doi.org/10.1152/physrev.00021.2018

13. Timmerman LA, Grego-Bessa J, Raya A, Bertrán E, Pérez-Pomares JM, Díez J, Aranda S, Palomo S, McCormick F, Izpisúa-Belmonte JC et al (2004) Notch promotes epithelial-mesenchymal transition during cardiac development and oncogenic transformation. Genes Dev 18(1):99–115. https://doi.org/10.1101/gad.276304

14. Niessen K, Fu Y, Chang L, Hoodless PA, McFadden D, Karsan A (2008) Slug is a direct Notch target required for initiation of cardiac cushion cellularization. J Cell Biol 182(2):315–25. https://doi.org/10.1083/jcb.200710067

15. Hinton RB, Yutzey KE (2011) Heart valve structure and function in development and disease. Annu Rev Physiol 73:29–46. https://doi.org/10.1146/annurev-physiol-012110-142145

16. Roberts WC, Ko JM (2005) Frequency by decades of unicuspid, bicuspid, and tricuspid aortic valves in adults having isolated aortic valve replacement for aortic stenosis, with or without associated aortic regurgitation. Circulation 111(7):920–925. https://doi.org/10.1161/01.Cir.0000155623.48408.C5

17. Armstrong EJ, Bischoff J (2004) Heart valve development: endothelial cell signaling and differentiation. Circ Res 95(5):459–70. https://doi.org/10.1161/01.RES.0000141146.95728.da

18. Bruneau BG (2008) The developmental genetics of congenital heart disease. Nature 451(7181):943–948. https://doi.org/10.1038/nature06801

19. LaHaye S, Lincoln J, Garg V (2014) Genetics of valvular heart disease. Curr Cardiol Rep 16(6):487. https://doi.org/10.1007/s11886-014-0487-2

20. Garg V, Kathiriya IS, Barnes R, Schluterman MK, King IN, Butler CA, Rothrock CR, Eapen RS, Hirayama-Yamada K, Joo K et al (2003) GATA4 mutations cause human congenital heart defects and reveal an interaction with TBX5. Nature 424(6947):443–7. https://doi.org/10.1038/nature01827

21. Okubo A, Miyoshi O, Baba K, Takagi M, Tsukamoto K, Kinoshita A, Yoshiura K, Kishino T, Ohta T, Niikawa N et al (2004) A novel GATA4 mutation completely segregated with atrial septal defect in a large Japanese family. J Med Genet 41(7):e97. https://doi.org/10.1136/jmg.2004.018895

22. Xiang R, Fan LL, Huang H, Cao BB, Li XP, Peng DQ, Xia K (2014) A novel mutation of GATA4 (K319E) is responsible for familial atrial septal defect and pulmonary valve stenosis. Gene 534(2):320–3

23. Misra C, Sachan N, McNally CR, Koenig SN, Nichols HA, Guggilam A, Lucchesi PA, Pu WT, Srivastava D, Garg V (2012) Congenital heart disease-causing Gata4 mutation displays functional deficits in vivo. PLoS Genet 8(5):e1002690. https://doi.org/10.1371/journal.pgen.1002690

24. Foffa I, Ait Alì L, Panesi P, Mariani M, Festa P, Botto N, Vecoli C, Andreassi MG (2013) Sequencing of NOTCH1, GATA5, TGFBR1 and TGFBR2 genes in familial cases of bicuspid aortic valve. BMC Med Genet 14:44. https://doi.org/10.1186/1471-2350-14-44

25. McKellar SH, Tester DJ, Yagubyan M, Majumdar R, Ackerman MJ, Sundt TM 3rd (2007) Novel NOTCH1 mutations in patients with bicuspid aortic valve disease and thoracic aortic aneurysms. J Thorac Cardiovasc Surg 134(2):290–6. https://doi.org/10.1016/j.jtcvs.2007.02.041

26. Mohamed SA, Aherrahrou Z, Liptau H, Erasmi AW, Hagemann C, Wrobel S, Borzym K, Schunkert H, Sievers HH, Erdmann J (2006) Novel missense mutations (p.T596M and p.P1797H) in NOTCH1 in patients with bicuspid aortic valve. Biochem Biophys Res Commun 345(4):1460–5. https://doi.org/10.1016/j.bbrc.2006.05.046

27. Laforest B, Andelfinger G, Nemer M (2011) Loss of Gata5 in mice leads to bicuspid aortic valve. J Clin Invest 121(7):2876–87. https://doi.org/10.1172/jci44555

28. Galvin KM, Donovan MJ, Lynch CA, Meyer RI, Paul RJ, Lorenz JN, Fairchild-Huntress V, Dixon KL, Dunmore JH, Gimbrone MAJR et al (2000) A role for smad6 in development and homeostasis of the cardiovascular system. Nat Genet 24(2):171–4. https://doi.org/10.1038/72835

29. Tan HL, Glen E, Töpf A, Hall D, O'Sullivan JJ, Sneddon L, Wren C, Avery P, Lewis RJ, ten Dijke P et al (2012) Nonsynonymous variants in the SMAD6 gene predispose to congenital cardiovascular malformation. Hum Mutat 33(4):720–7. https://doi.org/10.1002/humu.22030

30. Okajima T, Irvine KD (2002) Regulation of notch signaling by o-linked fucose. Cell 111(6):893–904. https://doi.org/10.1016/s0092-8674(02)01114-5

31. Shao L, Moloney DJ, Haltiwanger R (2003) Fringe modifies O-fucose on mouse Notch1 at epidermal growth factor-like repeats within the ligand-binding site and the Abruptex region. J Biol Chem 278(10):7775–82. https://doi.org/10.1074/jbc.M212221200

32. Mugisha S, Di X, Disoma C, Jiang H, Zhang S (2022) Fringe family genes and their modulation of Notch signaling in cancer. Biochim Biophys Acta Rev Cancer 1877(4):188746. https://doi.org/10.1016/j.bbcan.2022.188746

33. D'Amato G, Luxán G, del Monte-Nieto G, Martínez-Poveda B, Torroja C, Walter W, Bochter MS, Benedito R, Cole S, Martinez F et al (2016) Sequential Notch activation regulates ventricular chamber development. Nat Cell Biol 18(1):7–20. https://doi.org/10.1038/ncb3280

34. Panin VM, Papayannopoulos V, Wilson R, Irvine KD (1997) Fringe modulates Notch-ligand interactions. Nature 387(6636):908–12. https://doi.org/10.1038/43191

35. Munro S, Freeman M (2000) The notch signalling regulator fringe acts in the Golgi apparatus and requires the glycosyltransferase signature motif DXD. Curr Biol 10(14):813–20. https://doi.org/10.1016/s0960-9822(00)00578-9

36. Sethi MK, Buettner FF, Krylov VB, Takeuchi H, Nifantiev NE, Haltiwanger RS, Gerardy-Schahn R, Bakker H (2010) Identification of glycosyltransferase 8 family members as xylosyltransferases acting on O-glucosylated notch epidermal growth factor repeats. J Biol Chem 285(3):1582–6. https://doi.org/10.1074/jbc.C109.065409

37. Rana NA, Haltiwanger RS (2011) Fringe benefits: functional and structural impacts of O-glycosylation on the extracellular domain of Notch receptors. Curr Opin Struct Biol 21(5):583–9. https://doi.org/10.1016/j.sbi.2011.08.008

38. Moloney DJ, Panin VM, Johnston SH, Chen J, Shao L, Wilson R, Wang Y, Stanley P, Irvine KD, Haltiwanger RS et al (2000) Fringe is a glycosyltransferase that modifies Notch. Nature 406(6794):369–375. https://doi.org/10.1038/35019000

39. Travisano SI, Oliveira VL, Prados B, Grego-Bessa J, Piñeiro-Sabarís R, Bou V, Gómez MJ, Sánchez-Cabo F, MacGrogan D, de la Pompa JL (2019) Coronary arterial development is regulated by a Dll4-Jag1-EphrinB2 signaling cascade. Elife 8:e49977. https://doi.org/10.7554/eLife.49977

40. MacGrogan D, D'Amato G, Travisano S, Martinez-Poveda B, Luxán G, Del Monte-Nieto G, Papoutsi T, Sbroggio M, Bou V, Gomez-Del Arco P et al (2016) Sequential ligand-dependent notch signaling activation regulates valve primordium formation and morphogenesis. Circ Res 118(10):1480–97. https://doi.org/10.1161/circresaha.115.308077

41. Garside VC, Chang AC, Karsan A, Hoodless PA (2013) Coordinating Notch, BMP, and TGF-β signaling during heart valve development. Cell Mol Life Sci 70(16):2899–917. https://doi.org/10.1007/s00018-012-1197-9

42. Gonzalez DM, Medici D (2014) Signaling mechanisms of the epithelial-mesenchymal transition. Sci Signal 7(344):re8. https://doi.org/10.1126/scisignal.2005189

43. MacGrogan D, Münch J, de la Pompa JL (2018) Notch and interacting signalling pathways in cardiac development, disease, and regeneration. Nat Rev Cardiol 15(11):685–704. https://doi.org/10.1038/s41569-018-0100-2

44. Beis D, Bartman T, Jin SW, Scott IC, D'Amico LA, Ober EA, Verkade H, Frantsve J, Field HA, Wehman A et al (2005) Genetic and cellular analyses of zebrafish atrioventricular cushion and valve development. Development 132(18):4193–4204. https://doi.org/10.1242/dev.01970

45. Paige SL, Thomas S, Stoick-Cooper CL, Wang H, Maves L, Sandstrom R, Pabon L, Reinecke H, Pratt G, Keller G et al (2012) A temporal chromatin signature in human embryonic stem cells identifies regulators of cardiac development. Cell 151(1):221–32. https://doi.org/10.1016/j.cell.2012.08.027

46. Cai C, Sang C, Du J, Jia H, Tu J, Wan Q, Bao B, Xie S, Huang Y, Li A et al (2019) Knockout of tnni1b in zebrafish causes defects in atrioventricular valve development via the inhibition of the myocardial wnt signaling pathway. Faseb J 33(1):696–710. https://doi.org/10.1096/fj.201800481RR

47. Laurent F, Girdziusaite A, Gamart J, Barozzi I, Osterwalder M, Akiyama JA, Lincoln J, Lopez-Rios J, Visel A, Zuniga A et al (2017) HAND2 target gene regulatory networks control atrioventricular canal and cardiac valve development. Cell Rep 19(8):1602–1613. https://doi.org/10.1016/j.celrep.2017.05.004

48. Bi Y, Yang Z, Jin M, Zhai K, Wang J, Mao Y, Liu Y, Ding M, Wang H, Wang F et al (2022) ERp44 is required for endocardial cushion development by regulating VEGFA secretion in myocardium. Cell Prolif 55(3):e13179. https://doi.org/10.1111/cpr.13179

49. Liu Y, Lu X, Xiang FL, Lu M, Feng Q (2013) Nitric oxide synthase-3 promotes embryonic development of atrioventricular valves. PLoS One 8(10):e77611. https://doi.org/10.1371/journal.pone.0077611

50. Haines N, Irvine KD (2003) Glycosylation regulates Notch signalling. Nat Rev Mol Cell Biol 4(10):786–97. https://doi.org/10.1038/nrm1228

Publisher's Note Springer Nature remains neutral with regard to jurisdictional claims in published maps and institutional affiliations.

Authors and Affiliations

Junjie Yang[1,2] · **Zhi Wang**[2] · **Yue Zhou**[2] · **Shiwei Jiang**[2] · **Xiji Qin**[2] · **Zhikang Xu**[2] · **Yu Wang**[1,2] · **Mengying Zuo**[2,3] · **Zhuo Meng**[2] · **Sun Chen**[2] · **Qingjie Wang**[2] · **Jian Wang**[2] · **Kun Sun**[1,2] ⓘ

✉ Qingjie Wang
wangqingjie@xinhuamed.com.cn

✉ Jian Wang
wangjian@xinhuamed.com.cn

✉ Kun Sun
sunkun@xinhuamed.com.cn

[1] Department of Pediatric Cardiology, The Second Affiliated Hospital, Yuying Children's Hospital of Wenzhou Medical University, Wenzhou, China

[2] Department of Pediatric Cardiology, School of Medicine, Xinhua Hospital, Shanghai Jiao Tong University, Shanghai, China

[3] Department of Cardiology, Children's Hospital of Soochow University, Suzhou, China